

Photochemical & Photobiological Sciences

Accepted Manuscript



This is an *Accepted Manuscript*, which has been through the Royal Society of Chemistry peer review process and has been accepted for publication.

Accepted Manuscripts are published online shortly after acceptance, before technical editing, formatting and proof reading. Using this free service, authors can make their results available to the community, in citable form, before we publish the edited article. We will replace this *Accepted Manuscript* with the edited and formatted *Advance Article* as soon as it is available.

You can find more information about *Accepted Manuscripts* in the [Information for Authors](#).

Please note that technical editing may introduce minor changes to the text and/or graphics, which may alter content. The journal's standard [Terms & Conditions](#) and the [Ethical guidelines](#) still apply. In no event shall the Royal Society of Chemistry be held responsible for any errors or omissions in this *Accepted Manuscript* or any consequences arising from the use of any information it contains.

PAMAM G4.5-Chlorin e6 dendrimeric nanoparticles for enhanced photodynamic effect

Estelle Bastien^{1,2,3}, Raphaël Schneider⁴, Steffen Hackbarth⁵, Dominique Dumas⁶, Jordane Jasniewski⁷, Beate Röder⁵, Lina Bezdetsnaya^{1,2,3} and Henri-Pierre Lassalle^{1,2,3}

¹Université de Lorraine, Centre de Recherche en Automatique de Nancy, Campus Sciences, Vandœuvre-lès-Nancy, France

²Centre National de la Recherche Scientifique, Centre de Recherche en Automatique de Nancy, France

³Research Department, Institut de Cancérologie de Lorraine, Avenue de Bourgogne, 54519 Vandœuvre-lès-Nancy, France

⁴Université de Lorraine, Laboratoire Réactions et Génie des Procédés (LRGP), UMR 7274, CNRS, 1 rue Grandville, BP 20451, 54001 Nancy Cedex, France

⁵Institut für Physik, Humboldt, Universität zu Berlin, Newtonstrasse, Berlin, Germany

⁶Université de Lorraine, Plateforme IBISA d'Imagerie et de Biophysique Cellulaire de Nancy, Centre National de la Recherche Scientifique, Vandœuvre-lès-Nancy, France

⁷Université de Lorraine, Laboratoire d'ingénierie des biomolécules (LIBio), 2 avenue de la Forêt de Haye, Vandœuvre-lès-Nancy, France.

Abstract

There is currently great interest in the development of efficient and specific carrier delivery platforms for systemic photodynamic therapy. Therefore, we aimed to develop covalent conjugates between the photosensitizer chlorin e6 (Ce6) and PAMAM G4.5 dendrimers. The singlet oxygen generation (SOG) efficiency and fluorescence emission were moderately affected by the covalent binding of the Ce6 to the dendrimer. Compared to free Ce6, PAMAM anchored Ce6 display a much higher photodynamic effect, which is ascribable to better internalization in tumor cell model. Intracellular fate and internalization pathway of our different compounds were investigated using specific inhibition conditions and confocal fluorescence microscopy. Free Ce6 was shown to enter the cells by a simple diffusion mechanism, while G4.5-Ce6-PEG internalization was dependent of the caveolae pathway, whereas G4.5-Ce6 was subjected to the clathrin-mediated endocytosis pathway. Subcellular localization of PAMAM anchored Ce6, PEGylated or not, was very similar suggesting that the nanoparticles behave similarly in the cells. As a conclusion, we have demonstrated that PEGylated G4.5 PAMAM-Ce6 dendrimers may offer an effective furtive biocompatible nanoparticle for improved photodynamic treatment in preclinical tumor model.

Introduction

Photodynamic therapy (PDT) is a minimally-invasive photochemical-based approach that uses a combination of a light-activated drug (photosensitizer, PS) and the light of a specific wavelength to damage the target tumor tissue by generating reactive oxygen species¹. Among them, molecular oxygen in its first excited electronic state, so called singlet oxygen ($^1\text{O}_2$), is commonly agreed to be the cytotoxic key agent in photodynamic action. PDT has a clinical reality since several photosensitizers obtained an approval for the treatment of localized and light-accessible tumors.

For safe and effective therapy with limited side effects, PS should reach targeted cells at certain concentration threshold together with a low accumulation in healthy cells. However, to achieve this goal, two major problems are often encountered. Firstly, most PS molecules are hydrophobic and aggregate easily in aqueous media, resulting in reduced singlet oxygen generation¹ and difficulties with intravenous delivery². Secondly, PSs generally display a low or moderate selectivity to cancer cells, thus requiring high PS concentrations in clinical protocols, yielding serious adverse effects. To overcome these drawbacks, the use of vectors for PS tumors targeting was suggested, providing an improvement in PS solubility, protecting from PS deactivation reactions and favoring tumor targeting through the enhanced permeability and retention (EPR) effect. EPR is inherent to many solid tumors due to leaky vasculature and poor lymphatic drainage³. Currently basic research in PDT focuses mainly on the development of carrier systems for targeting tumor tissue⁴. To this aim, biocompatible nanocarriers for PS delivery such as lipid-based nanoparticles (NP)^{5,6}, polymer-based NPs^{7,8}, micelles^{9,10} or silica-based NPs¹¹, have been designed.

Dendrimers have been proposed as building blocks for PDT drug delivery systems already in 2001¹². Dendrimers are regular hyperbranched macromolecules of a few nanometers in size (2-10 nm) with many functional groups at their surface which allow anchoring therapeutic

molecules such as photosensitizers, stealth elements (polyethylene glycol), or targeting moieties on their surface, while controlling size and lipophilicity of the carrier. Given their low cytotoxicity and their water solubility many types of poly(amido amine) (PAMAM) dendrimers appear as a very attractive class of biocompatible nanovectors for drug targeting in cells and tissues¹³⁻¹⁵.

So far, three different assemblies of dendrimer-based carrier systems have been reported in the field of PDT. The first uses a porphyrin or phthalocyanine as starting core with a dendron grafted on each pyrrole unit. The Kataoka group reported good photodynamic efficacy of these NPs excitable in the far red, making them eligible for *in vivo* applications^{16, 17}. The second construction consists of photosensitizers like protoporphyrin IX (PpIX) encapsulated in the dendrimer, which can be progressively released into the medium¹⁸. The last class of structures is based on the covalent binding of PS on the periphery groups of dendrimers. As we recently demonstrated PpIX prodrug, ALA (5-aminolaevulinic acid), can be attached to dendrimers via a cleavable ester bond, resulting in a higher synthesis rate and better tumor selectivity of PpIX *in vivo* compared with free ALA¹⁹. Hackbarth *et al.*¹² achieved an average loading of 12-13 molecules of pheophorbide a (Pheo) to one diaminobutane (DAB) dendrimer molecule with 16 available binding sites. However, singlet oxygen generation of covalently linked dye molecules was dramatically reduced compared with free Pheo, mostly due to trap formation (excitonic interaction of at least two neighboring chromophores) combined with Förster-energy transfer between different Pheo molecules at the surface of highly loaded dendrimer. Strong quenching effects were also reported for high loaded peryleneimide-terrylenediimide polyphenyl dendrimers^{12, 20}.

The present paper evaluates the therapeutic *in vitro* efficiency of the photoactive NP consisting of the PS Chlorin e6 (Ce6) covalently bound to biocompatible PAMAM G4.5 dendrimer. To avoid strong quenching effect, only 25% of the carboxylic acid groups present

at the dendrimer surface were modified with the PS. Herein, we describe the photophysical properties, subcellular localization and internalization pathway of Ce6-grafted dendrimers (G4.5-Ce6). Changes observed in cellular uptake and phototoxicity upon PEGylation of the NPs were also evaluated.

Experimental

Materials and general procedure

Starburst polyamidoamine (PAMAM) dendrimer generation 4.5 (5 wt% in methanol, containing 128 surface carboxylate groups, MW 26228 g.mol⁻¹), benzotriazole-1-yl-oxy-tris-(dimethylamino)phosphonium hexafluorophosphate (BOP), poly(ethylene glycol) methyl ether (MW 2000 g.mol⁻¹), dicyclohexylcarbodiimide (DCC), 4-dimethylaminopyridine (DMAP), N-hydroxysuccinimide (NHS), diisopropylethylamine (DIPEA), 2,2'-(ethylenedioxy)bis(ethylamine), trifluoroacetic acid (TFA), chlorpromazine, genistein, 5-(N-ethyl-N-isopropyl) amiloride (EIPA), DMSO, MeOH and dichloromethane were purchased from Sigma-Aldrich (St Louis, MO, USA). Chlorin e6 (Ce6) was purchased from Livchem (Frankfurt, Germany). RPMI 1640 medium, L-glutamine, foetal bovine serum, penicillin-streptomycin and phosphate-buffered saline (PBS) were supplied by GibcoBRL (Merelbeke, Belgium). Ultrapure water was used through all experiments. All starting materials and organic solvents were directly used without further purification. N-Boc-protected 2,2'-(ethylenedioxy)bis(ethylamine) was prepared according to Trester-Zedlitz²¹.

Synthesis of Chlorin e6 - PAMAM dendrimer nanoparticles.

Coupling of Ce6 with N-Boc-protected 2,2'-(ethylenedioxy)bis(ethylamine).

Under argon atmosphere in darkness, Ce6 (100 mg, 1.677 10⁻⁴ mol) was dissolved in 58 mL of anhydrous CH₂Cl₂. DCC (34.6 mg, 1.677 10⁻⁴ mol) and DMAP (4 mg, 3.27 10⁻⁵ mol) were

added to the Ce6 solution and the mixture stirred for 10 min at room temperature. Separately, N-Boc-protected 2,2'-(ethylenedioxy)bis(ethylamine) (50 mg, $2.012 \cdot 10^{-4}$ mol) and DIPEA (26 mg, $2.012 \cdot 10^{-4}$ mol) were dissolved in 10 mL CH_2Cl_2 . This solution was added to the activated Ce6 and the mixture stirred at room temperature for 10 h. The progress of the reaction was monitored by thin layer chromatography using MeOH/ CH_2Cl_2 (10:90) as eluent. The precipitant dicyclohexylurea was removed by filtration through a glass filter. The reaction mixture was then poured into a separation funnel, washed with water (25 mL), saturated brine (25 mL), dried over Na_2SO_4 and the solvent evaporated under reduced pressure. Compound **1** (Scheme 1) was isolated in 82% yield after column chromatography on silica gel using MeOH/ CH_2Cl_2 (10:90) as eluent.

Deprotection of the BOC group. Synthesis of compound 2.

In the dark under an argon atmosphere, compound **1** (100 mg, $1.187 \cdot 10^{-4}$ mol) was treated with TFA/ CH_2Cl_2 (1:1, 7 mL) at room temperature. After being stirred for 2 h, TFA and CH_2Cl_2 were evaporated. The residue was taken up in CH_2Cl_2 (30 mL) and stirred with K_2CO_3 . After filtration, the organic layer was concentrated under reduced pressure and compound **2** was obtained in 96% yield. Chlorin **2** (Scheme 1) was used without further purification for the next step.

Anchorage of 2 at the surface of G4.5 PAMAM dendrimer.

The anchorage of **2** at the surface of G4.5 PAMAM dendrimer (Scheme 2) was conducted according to a synthetic procedure described by Hargus et al. with slight modifications²². Briefly, methanol was first evaporated in vacuo from the commercial G4.5 PAMAM dendrimer solution. The obtained oil (235 mg, $8.95 \cdot 10^{-6}$ mol) was solubilized in anhydrous DMSO (10 mL). DCC (118.2 mg, $5.73 \cdot 10^{-4}$ mol) and NHS (98.91 mg, $8.585 \cdot 10^{-4}$ mol) were then added to activate surface carboxylate functions and the solution was stirred for 15 h at room temperature under argon atmosphere. Chlorin **2** (0.187 mg, $2.57 \cdot 10^{-4}$ mol) in 10 mL

DMSO was then added and the mixture stirred for 24 h. The precipitant dicyclohexylurea was removed by filtration through a glass filter. The reaction medium was then diluted with water (50 mL) and dialyzed using a dialysis bag (molecular weight of 6-8000 Da cut off) against ultrapure water for 72 h, the water being changed every 24 h, to remove low MW contaminants and unreacted **2**. The solution was finally lyophilized to provide pure **3** in 91% yield. Attachment of **2** to the dendrimer provided exclusively compound **3**, requiring only a dialysis for workup, thus facilitating scale up (Scheme 2).

Surface PEGylation of 3.

Finally, in order to increase the blood circulation times and the accumulation in tumor tissue, poly(ethylene glycol) methyl ether (mPEG₂₀₀₀-OMe, MW 2000) was used to cover ca. 8% of the carboxylic groups on the surface of the periphery of dendrimer **3** (Scheme 3).

Surface PEGylation of **3** was achieved by formation of ester bonds between surface carboxylate groups of the dendrimer and poly(ethylene glycol) methyl ether (MW 2000, mPEG₂₀₀₀-OMe) using BOP as a coupling agent and methanol as a solvent²³. Under argon and in the dark, compound **3** (0.180 g, 4.08 10⁻⁶ mol) and BOP (0.086 g, 1.95 10⁻⁴ mol) were dissolved in 20 mL anhydrous methanol. mPEG₂₀₀₀-OMe (0.130 g, 6.537 10⁻⁵ mol) was then added and the mixture was stirred for 3 days at room temperature. Methanol was next evaporated *in vacuo*. The residue was solubilized in water (30 mL) and dialyzed using a dialysis bag (molecular weight 6-8000 cut off) against ultrapure water for 48 h, the water being changed every 24 h, to remove low MW contaminants and unreacted mPEG₂₀₀₀-OMe without significant lowering of the yield of the PEGylated dendrimer. The solution was finally lyophilized to provide compound **4**.

Characterization.

The Ce6 concentration of G4.5-Ce6 (+/-PEG) solution was determined by UV/Vis spectroscopy (Lambda 35 UV/Vis spectrofluorimeter LS55 PerkinElmer). Free Ce6 was dissolved in ethanol at different concentrations to generate a standard curve and calculate the molar extinction coefficient at 665 nm. The amount of Ce6 content in PAMAM G4.5 solution was calculated assuming the same extinction coefficient as for Ce6 in solution. Fluorescence spectra of free Ce6 and G4.5-Ce6 (+/- PEG) were recorded using an LS55 fluorescence spectrometer (Perkin Elmer). All measurements were done in ethanol at the dye concentration of 0.5 $\mu\text{g/mL}$; at this dye concentration the optical density did not exceed 0.1 at $\lambda_{\text{exc}} = 410$ nm. Hydrodynamic diameter and zeta potential of G4.5-Ce6 and G4.5-Ce6-PEG NP were determined using Malvern Zetasizer Nano ZS (173°, 532 nm, 25°C). The sample were prepared at a concentration of 1 $\mu\text{g/mL}$ in water milliQ and filtered at 0.1 μm . Hydrodynamic diameter is reported as the volume-weighted average of twelve measurements.

For zeta potentials a voltage of 100V was applied at 25°C. Samples were loaded into pre-rinsed folded capillary cells; at least three independent measurements were made.

Evaluation of the singlet oxygen generation (SOG).

Singlet oxygen luminescence kinetics have been recorded using time correlated multi photon counting employing the NIR PMT H10330-45 from Hamamatsu as detector. The setup is identical to the $^1\text{O}_2$ luminescence detection system TCMPC1270 of SHB Analytics, Germany. The excitation intensity profile, temporal shape and spectrum of the pulsed LED excitation around 400 nm are given in Hackbarth *et al.*²⁴. The optical density of the samples and reference is adjusted to 0.1 at 400 nm. Singlet oxygen quantum yield of the reference substance (5,10,15,20-tetrakis(N-methyl-4-pyridyl)-21H,23H-porphine, TMPyP) was

previously measured to be 0.70 ± 0.05 in ethanol. This value is consistent with the value reported earlier by Wilkinson *et al.*²⁵.

Cell culture.

Human pharynx squamous cell carcinoma (FaDu) cell line was obtained from the American Type Culture Collection (ATCC[®] HTB-43[™]). FaDu were grown in humidified incubator at 37°C, 5% CO₂, in RPMI 1640 medium (Roswell Park Memorial Institute) supplemented with 10% fetal bovine serum (FBS), 1% penicillin-streptomycin and 1% L-glutamine.

***In vitro* photocytotoxicity assessed by clonogenic assay.**

Cells were seeded into 6-wells plates at a concentration of 9.10^4 cells per well. Following incubation for 48h, the cells were washed with PBS and incubated for 24h in RPMI supplemented with 2% FBS and containing each compound at varying concentrations. Stock solution of Ce6 was prepared in DMSO so that the concentration of solvent never exceeded 0.1% in the medium. G4.5-Ce6 (+/-PEG) was prepared in water. After two consecutive washings with PBS, fresh medium was added and cells were irradiated at 652 nm with a Ceralas PDT diode laser (CeramOptec GmbH, Bonn, Germany) at a fluence of 2.5 J.cm^{-2} with a fluence rate of 10 mW.cm^{-2} . The cell viability was then evaluated by clonogenic assay. The cells were washed and incubated with trypsin-EDTA to make single-cell suspensions from monolayer cultures. Viable cells were then seeded in 6-well plate at a concentration of 500 cells/well. Ten days later, the culture medium was removed and cells were washed and incubated 5 min at room temperature successively with 70% ethanol and 1% crystal violet solution. Then the colonies were washed and counted. Results are given as percentage of survival cells normalized to those obtained from control groups (drug, no light). To determine

the dark toxicity of the compounds, well plates were prepared in the same manner as described above without irradiation.

Cellular uptake assay.

FaDu cells ($3 \cdot 10^4$ cells/well) were seeded in 24-well plates, 48 h later the cells were washed with PBS and incubated for 24h in RPMI supplemented with 2% FBS and containing each compound under investigation at varying concentrations. After three consecutive washings with PBS, SolvableTM (PerkinElmer) was added for 2h at 50°C for solubilizing cells. The cellular uptake of Ce6 was determined from fluorescence calibration curves constructed by plotting the peak height of Ce6 standard solutions in SolvableTM. The calibration was linear within this range. Error bars are the standard deviation for three independent experiments.

Internalization pathway inhibition studies.

FaDu cells ($3 \cdot 10^4$ cells/well) were seeded in 24-well plates, and incubated for 48h prior to the addition of NPs. Then, the cells were pre-incubated in RPMI 2% FBS for 30 min with either 10 $\mu\text{g} \cdot \text{ml}^{-1}$ Chlorpromazine (inhibitor of clathrin-dependent endocytosis), 400 μM Genistein (inhibitor of caveolae-dependent endocytosis) and 100 μM EIPA (inhibitor of macropinocytosis). The impact of low temperature was studied by pre-incubating cells at 4°C for 30 min prior to exposure to the compounds. After this pre-incubation, G4.5-Ce6(+/- PEG) (final concentration 0.5 $\mu\text{g} \cdot \text{ml}^{-1}$) were added and incubated for 60 min, either in the presence of the inhibitors or at 4°C. Ce6 uptake was measured as previously described. Results are given as percentage of uptake normalized to those obtained from control groups (without inhibitors or at 37°C).

Subcellular localization of NP with or without PEG.

FaDu cells (1.10^4 cells. ml^{-1}) were plated into four well chambers Slideflask (Nunc, Roskilde, Denmark), incubated in the dark at 37°C with $2 \mu\text{g ml}^{-1}$ of free Ce6 or NP-Ce6 (+/- PEG) during 24 h, then rinsed and incubated with organelles specific fluorescent probes. The ER was labelled with DiOC₆ dye, applied for 1 min at a final concentration of 2.5 mg ml^{-1} . To identify Golgi apparatus, cells were labelled with $5 \cdot 10^6$ M of NBD-C₆ ceramide for 30 min at 4°C , then rinsed with cold PBS solution and re-incubated in the RPMI 9% FBS at 37°C for the next 30 min. The staining of mitochondria and lysosome was performed by cells incubation with $2 \cdot 10^{-7}$ M of MitoTracker[®] Green or $7.5 \cdot 10^{-8}$ M of LysoTracker[®] Green for 30 min at 37°C . Before observation, cells were washed with PBS to remove dyes. Double-stained cells were observed with a confocal laser-scanning microscope (Leica SP5 X AOBS LCSM; Leica microsystem, Wetzlar, Germany). A white light laser (SuperK, extreme supercontinuum lasers, NKT Photonics) was used to excite organelle specific fluorescent probes and Ce6 at appropriate wavelengths. Fluorescence emission of Ce6 (peak 665 nm) was collected from 645 to 690 nm on one channel (red), and fluorescence from organelle specific labelling was collected from 505 to 550 nm on a second channel (green), with the pinhole locked at 600 μm . A water immersion objective ($\times 63$) was used to capture each image of 1024×1024 pixels. No visible photobleaching was observed during image acquisition. Colocalization was quantified with Pearson's correlation coefficient (PCC). Absolute PCC values of 1-0.7 indicate a relatively strong correlation, 0.69-0.36 indicate a moderate correlation, 0.35-0.2 indicate a weak correlation, and <0.2 indicates the absence of a correlation^{26,27}. The square of PCC value represents the percentage of Ce6 fluorescence signal arising from the fluorescence of the organelle marker²⁶.

Fluorescence-lifetime imaging.

The cell images were observed with a CLSM (FluoView™ FV1000, Olympus) with FLIM-extension (Pico Quant, Berlin). Fluorophores were excited with a nanosecond pulse laser at $\lambda_{\text{ex}} = 440$ nm. FaDu cells were incubated 24h with G4.5-Ce6(+/- PEG) or free Ce6. After two consecutive washings with PBS, fresh medium was added and cells were analyzed by FLIM equipment before and after irradiation (white light 10 mW/cm²; 5 min).

Statistical analysis.

Statistical significance among two conditions was assessed using the nonparametric Mann-Whitney test. P-value was considered at the 5% level of significance to deduce inference of the significance of the data.

Results and Discussion

Physical and photophysical characterization

The hydrodynamic diameter determined by DLS (Table 1) is 6.3 nm for G4.5-Ce6 and 12 nm for G4.5-Ce6-PEG (PDI of 0.23 and 0.33, respectively). The surface charge exhibits a negative zeta potential of -17.7 mV and -8.9 mV for G4.5-Ce6 and G4.5-Ce6-PEG, respectively, due to the presence of the carboxylate functions at neutral pH.

Absorption and fluorescence spectra of free Ce6, G4.5-Ce6 and G4.5-Ce6-PEG are shown in Fig. 1. The covalent binding between Ce6 and the dendrimer results in slight changes in the absorption spectra. A small bathochromic shift of the lowest Q-band (2 nm) together with a moderate increase of the bandwidth of all the absorption bands are observed for the G4.5-Ce6 and G4.5-Ce6-PEG compared to free Ce6 (Table 1, Fig. 1a). Similar effects were previously observed for comparable nanohybrids¹² and have been attributed to local changes of the refractive index due to the vicinity of the PS to each other²⁸. This also indicates that the attached Ce6 molecules interact partly, without general aggregation or structure modification

when Ce6 was loaded with amide bonds on the PAMAM G4.5 dendrimers.

The fluorescence spectra of the NPs are very similar to Ce6 in ethanol solution (Fig. 1b), but the fluorescence quantum yield Φ_F is reduced after covalent binding (0.11 and 0.09 for G4.5-Ce6 and G4.5-Ce6-PEG, respectively) compared to free Ce6 (0.16)²⁹ (Table 1). The singlet oxygen quantum yield Φ_Δ is reduced to 0.31 and 0.26, for G4.5-Ce6 and G4.5-Ce6-PEG, respectively compared to free Ce6 (0.55). The statistical loading of Ce6 on the dendrimer results in different PS-PS distances. Few of them are close enough for an excitonic interaction, resulting in non-radiative deactivation of the excited singlet state. However, the majority of Ce6 molecules at the same dendrimer are obviously sufficiently isolated to avoid Forster transfer towards this PS pair. Therefore the probability of quenching is much lower compared to the dendrimers constructs reported in Hackbarth *et al.*¹². The Förster radius of Ce6 can be calculated as 23Å, while the average distance between PSs at one dendrimer is 22Å, when computed from the measured diameter of our G4.5-Ce6 dendrimer (6.3 nm, Table 1) and the average number of Ce6 molecules linked on the dendrimer (32). Due to the strong dependency of the distance between molecules on the FRET (factor of 10^6), variation in the distance of only 20% causes the molecule to behave like a monomer in solution or undergo nearly exclusively FRET resulting in quenching. Quenching of around 40%-50% (Table1) appears to be reasonable in this context.

Photodynamic activity and cellular uptake.

The viability of FaDu cells was evaluated by clonogenic assay in function of PSs concentration. No dark cytotoxicity was observed after treatment with Ce6, G4.5-Ce6 or G4.5-Ce6-PEG in the range of the tested concentrations (Fig. S1). However, when irradiated, both dendrimer based NPs showed a remarkable and concentration dependent phototoxicity (Fig. 2). The IC_{50} , defined as the concentration of PS at which 50% of tumor cells survive after photoirradiation are displayed in the inset of Fig. 2. The IC_{50} of free Ce6 after 24h incubation and irradiation (2.5 J.cm^{-2}) is $0.7 \mu\text{g.ml}^{-1}$ (Fig. 2). This value is consistent with other studies using Ce6 under similar irradiation conditions^{30, 31}. The IC_{50} of G4.5-Ce6 and G4.5-Ce6-PEG dendrimers were respectively 3 and 7 times lower ($0.1 \mu\text{g.ml}^{-1}$ and $0.3 \mu\text{g.ml}^{-1}$) (Fig. 2). The same order of IC_{50} was reported earlier for aryl ether dendrimer Zn-porphyrin complexes under similar experimental conditions³².

Ce6 cellular uptake was significantly enhanced once anchored at the surface of the dendrimer compared to free PS (Fig. 3). Independent of the incubation concentration, the mean uptake (slope of the uptake fitting line) is increased by a factor of 10 for G4.5-Ce6-PEG and a factor of 22 for G4.5-Ce6 compared to free Ce6. The G4.5-Ce6 demonstrated two-fold higher intracellular accumulation compared to G4.5-Ce6-PEG (Fig. 3). These results are consistent with several reports demonstrating that the presence of PEG chains negatively affect the uptake of the nanoparticles *in vitro*^{33, 34}. Besides avoiding aggregation and preventing an opsonization during blood circulation, the PEG layer decreases interactions between grafted chains and cell membrane leading to reduced cellular uptake³³, a phenomenon known as the “PEG dilemma”³⁵. The enhanced uptake of G4.5-Ce6 and G4.5-Ce6-PEG (Fig. 3) could be responsible for better photocytotoxicity of dendrimer-based compounds (Fig. 2). However if the phototoxicity is recalculated in terms of equivalent intracellular Ce6 concentration, it appears that the phototoxicity of NPs is 3 times less efficient compared to free Ce6. A major

part of this difference can be explained by the lower singlet oxygen quantum yield of the PAMAM G4.5-modified Ce6 (Table 1). Moreover, subcellular localization could be of importance too.

Subcellular localization

The effect of vectorization on the subcellular distribution of Ce6 was investigated by CLSM with specific organelles fluorescent probes. Co-staining of FaDu cells with LysoTracker shows that Ce6 once associated to dendrimers was strongly localized in the lysosomes, with a Pearson's Correlation Coefficient >0.7 (Fig. 4a and 4b). On the opposite, free Ce6 was not found in the lysosomes ($PCC < 0.35$) but distributed elsewhere in the cell. Co-staining of Ce6-based compounds Mitochondria, Golgi apparatus and the ER was performed with Mitotracker, NBD and DioC6 respectively (Fig. 4b, Fig. S2). All compounds had fairly the same localization pattern in these organelles, except G4.5-Ce6 which is strongly confined to Golgi apparatus while G4.5-Ce6-PEG and Ce6 were localized moderately in this organelle. As compared to ER or mitochondria, which are key organelles in the apoptotic cell death pathway, the PS localization in lysosomes is less favorable in terms of photocytotoxicity^{36, 37}. Thus, the next challenge could be the release of Ce6 from the dendrimer-based NP, paving the way to a further improvement of photoefficiency.

Internalization pathway and intracellular fate of the nanoconstructs.

Fig. 5 displays an uptake inhibition carried out by incubation of NPs with cells under different conditions. At 4°C, the internalization of Ce6 was unaffected, whereas the uptake of the two Ce6-dendrimers was lowered to 45% and 18% for G4.5-Ce6 and G4.5-Ce6-PEG, respectively. As energy-dependent cellular processes are inhibited at low temperature, we state that the free Ce6 internalization occurs via passive diffusion through the plasma

membrane, as has already been demonstrated in many studies³⁸⁻⁴¹. In opposite, the dendrimer NPs mainly enter the cells *via* an active transport process. The fluorescence signal of Ce6 dendrimers observable at 4°C could be attributed to diffusion or physical adhesion on the plasma membrane. This hypothesis is strengthened by the weaker internalization of PEGylated compared to non-PEGylated Ce6-dendrimers, most probably due to the well-known antifouling properties of the PEG layer⁴².

We further assessed the energy dependent internalization pathways as micropinocytosis, clathrin and caveolae uptake, using EIPA, chlorpromazine and Genistein respectively (Fig. 5). We did not observe any uptake inhibition of Ce6-dendrimers after EIPA treatment. Therefore, the macropinocytosis is not a major cell uptake mechanism for the Ce6-dendrimers NP as recently claimed by Yuan *et al.*⁴³. Clathrin-mediated endocytosis (CME) pathway is inherent solely to G4.5-Ce6, while PEGylated dendrimers were indifferent to chlorpromazine-mediated inhibition ($p > 0.05$). As reported by Shcharbin *et al.* with identical PAMAM dendrimers⁴⁴, serum components will be adsorbed at the surface of the G4.5-Ce6 to form a so called biomolecular corona⁴⁵, providing the receptor-ligand recognition, necessary for CME. On the other hand, the presence of PEG layer leads to a strong decrease of serum protein adsorption as demonstrated elsewhere^{46, 47}, and as such G4.5-Ce6-PEG dendrimers are insensitive to CME inhibition agent. Caveolae pathway endocytosis was assessed with genistein-mediated inhibition of Ce6 cellular uptake. Among both tested dendrimers, only uptake of the negatively charged G4.5-Ce6-PEG was mediated by caveolae receptor-independent endocytosis pathway. Consistent with our study, it has been reported that negatively charged COOH terminated PAMAM G3.5 dendrimers were endocytosed *via* the caveolae pathway⁴⁸.

Considering that G4.5-Ce6 and G4.5-Ce6-PEG display similar subcellular distribution pattern in the studied organelles, except that for Golgi apparatus (Fig. 4b), these results indicate that although the internalization mechanisms and uptake of Ce6-dendrimers were different, the presence of PEG had little impact on the intra-cellular fate of the corresponding dendrimer. Moreover, despite the different incorporation mechanisms between Ce6 and Ce6-dendrimer, we observed a linear uptake in function of PS concentration (Fig. 2). Considering the endocytosis NPs-mediated pathway, compared to diffusion transport for free Ce6, we expected the saturation of dendrimers uptake. In all probability, the plateau could not be reached in the range of tested concentrations ($0-2 \mu\text{g.mL}^{-1}$), while for higher concentrations a saturation of the uptake will definitely take place. Similar observation was reported earlier for gold nanoparticles⁴⁹.

Besides that, we have been interested in the Ce6 and Ce6-dendrimers uptake measured as a function of incubation time (see figure below). We could observe the plateau in NPs uptake but not for free Ce6. This shows that the incorporation of our NPs can be saturated.

Classically, molecules that are internalized by the clathrin pathway are known to be subjected to lysosomal degradation⁵⁰ as opposed to caveolae route which can avoid degradation⁵¹. However it has been shown in epithelial derived tumor cells that the caveolae and clathrin-mediated endocytosis pathways are connected and ends up in lysosomes⁵². Since FaDu cells belong to this category, it seems consistent that a certain proportion of the G4.5-Ce6-PEG is located in lysosomes.

Fluorescence Lifetime Imaging.

Fluorescence lifetime imaging data are presented in the Fig. 6. FaDu cells were incubated for 24h with either free Ce6 or G4.5-Ce6 NPs. FLIM is a valuable technique to study fluorophores properties in their microenvironment, such as photobleaching⁵³, aggregation

state⁵⁴ as well as their release from a NP⁵⁵. Fluorescence lifetimes (τ) were measured before and after cells irradiation with a light dose of 3 J.cm⁻². Before irradiation, τ values measured for G4.5-Ce6 and G4.5-Ce6-PEG were 5.1 ns and 4.9 ns, respectively, whereas it was significantly longer for free Ce6 (5.8 ns). After irradiation, lifetimes of G4.5-Ce6 NPs remain unchanged, while τ drops to 4.3 ns for free Ce6. Upon light irradiation, we observed a decrease of the fluorescence intensity for free Ce6, accompanied by a shortening of τ (Fig. 6). These changes for free Ce6, may be due to bleaching, relocalization or interaction with the local environment. However, no significant fluorescence lifetime changes were observed for G4.5-Ce6 and G4.5-Ce6-PEG, pointing out that Ce6 is not released from the dendrimer following irradiation.

Conclusion

PAMAM-Ce6 conjugates show a much higher photodynamic effect due to considerable internalization in tumor cell model compared to free Ce6. Free Ce6 was shown to enter the cells by a simple diffusion mechanism, while G4.5-Ce6 and G4.5-Ce6-PEG internalization was dependent of active endocytosis pathway. However, the nanoparticles behave similarly in the cells since their subcellular localization was comparable. As a result, PEGylated G4.5 PAMAM-Ce6 dendrimers may offer an effective furtive biocompatible nanoparticle for photodynamic treatment in preclinical tumor model. However, the reduced singlet oxygen quantum yield and pronounced localization in lysosomes indicate that great improvement of the photoefficiency of such nanoparticles is possible, if a release of the PS from the dendrimers after cellular uptake can be realized.

Acknowledgments

This work was supported by “Institut de Cancérologie de Lorraine” Research Funds, French “Ligue Nationale contre le Cancer (CCIR-GE)”, PHC Procope program (grant no. 31083XG) and “Région Lorraine”. The authors are grateful to Vairis Caune for the treatment of CLSM images.

Figure legends

Fig. 1: Absorption (a) and fluorescence emission (b) spectra of Ce6 (solid line), G4.5-Ce6 (dash line) and G4.5-Ce6-PEG (dot line) in ethanol. Ce6 concentration adapted to reach an OD of 0.1 in the Soret band.

Fig. 2: *In vitro* antitumor activity of free Ce6 (square), G4.5-Ce6 (round) and G4.5-Ce6-PEG (triangle) after photoirradiation (2.5 J.cm^{-2}). FaDu cells were treated 24h with various concentrations of free Ce6 or vectorized with G4.5 dendrimers (+/-PEG). IC_{50} : Concentration of the PS inducing 50% of cell death.

Fig. 3: Cellular uptake of free Ce6 (square), G4.5-Ce6 (round) and G4.5-Ce6-PEG (triangle) incubated with FaDu cells during 24h as function of the PS concentration.

Fig. 4a: CLSM images of lysosomal localization of Ce6, G4.5-Ce6 and G4.5-Ce6-PEG in FaDu cells. Left column display confocal overlay images. These micrographs were representative of those obtained from three independent experiments. Right column shows the mean Pearson's correlation diagram. Red color corresponds to Ce6 and green color corresponds to LysoTracker[®] Green. Bar = $10\mu\text{m}$.

Fig. 4b: Pearson's correlation coefficient (PCC) values quantifying the co-localization of the organelles fluorescent marker and free Ce6, G4.5-Ce6 or G4.5-Ce6-PEG in FaDu cells 24 h after incubation. PCC values of 1-0.7 indicate a relatively strong correlation, 0.69-0.36 indicate a moderate correlation, 0.35-0.2 indicate a weak correlation, and <0.2 indicates the absence of a correlation^{26,27}. (* $p < 0.05$ versus the free Ce6 group).

Fig. 5: Effect of various endocytosis inhibitors on cellular uptake of the PSs. FaDu cells were pre-incubated for 30 min at 4°C without the endocytosis inhibitors or at 37°C with inhibitors. After pre-incubation, PSs (final concentration $0.5 \mu\text{g.ml}^{-1}$) were added and incubated for 60 min, either in the presence of the inhibitors or at 4°C . (* $p < 0.05$ versus the untreated control group).

Fig. 6: Representation of fluorescence lifetime imaging microscopy (FLIM). FaDu cells were treated with $3 \mu\text{M}$ of free Ce6, G4.5-Ce6 or G4.5-Ce6-PEG. After 24h, the cells were observed under a fluorescence-lifetime imaging microscope before and after irradiation (a). Average fluorescence lifetimes for each PSs were determined (b).

Scheme 1: Synthetic route for the preparation of diamino PEG-functionalized chlorin 2.

Scheme 2: Synthetic route to multifunctional PAMAM dendritic NPs 3 and 4.

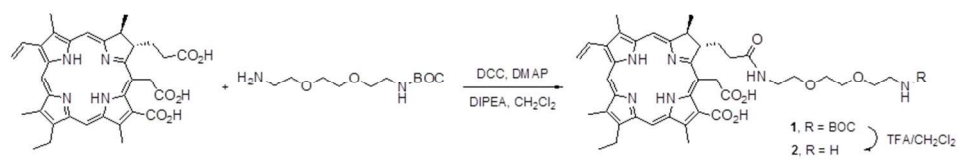
Fig. S1: *In vitro* dark cytotoxicity of free Ce6 (a), G4.5-Ce6 (b) and G4.5-Ce6-PEG (c). FaDu cells were treated 24h with various concentrations of free Ce6 or vectorized on G4.5 dendrimers (+/-PEG).

Fig. S2: CLSM images of subcellular distribution of DioC₆, Mitotracker and NBD-C₆ for free Ce6 (a), G4.5-Ce6 (b) and G4.5-Ce6-PEG (c) in FaDu cells. Red color corresponds to PS, green color corresponds to organelles probes and yellow color matches the colocalization. Right column shows the Pearson's correlation diagram. These micrographs were representative of those obtained from three independent experiments. Bar, 10µm

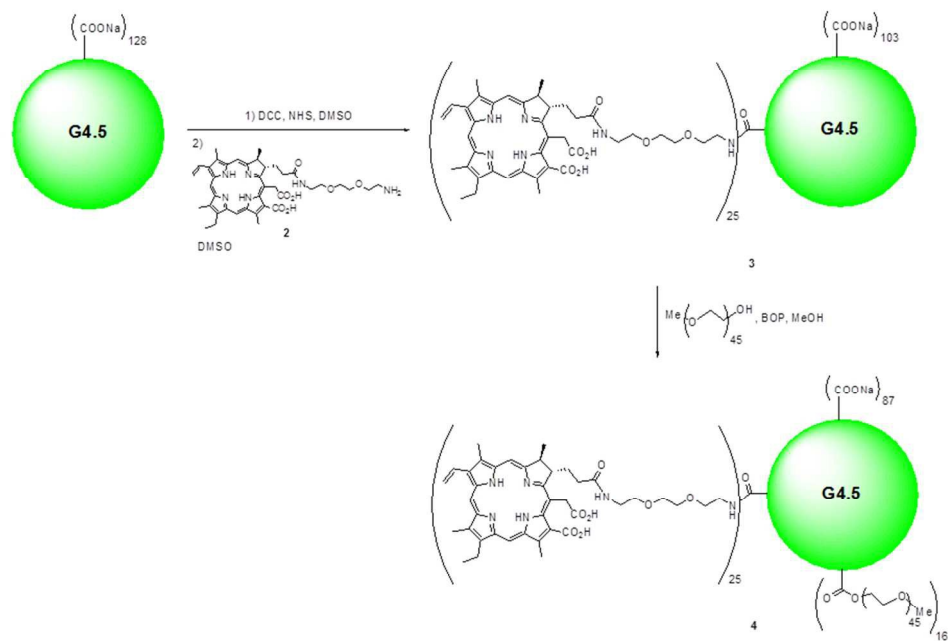
References

1. N. Kuznetsova, N. Gretsova, V. Derkacheva, O. Kaliya and E. Lukyanets, *J. Porphyrins Phthalocyanines*, 2003, **7**, 147-154.
2. T. Trindade, P. O'Brien and N. Pickett, *Chem. Mater.*, 2001, **13**, 3843-3858.
3. V. Torchilin, *Adv Drug Deliv Rev*, 2011, **63**, 131-135.
4. N. Jux and B. Röder, in *Handbook of Porphyrin Science*, eds. K. Kadish, K. Smith and R. Guilard, World Scientific Publishing Co. Pte. Ltd., Singapore, 2010, vol. 4, pp. 327-401.
5. H. P. Lassalle, D. Dumas, S. Grafe, M. A. D'Hallewin, F. Guillemin and L. Bezdetsnaya, *J Control Release*, 2009, **134**, 118-124.
6. A. S. Derycke and P. A. de Witte, *Adv Drug Deliv Rev*, 2004, **56**, 17-30.
7. A. Preuss, S. Hackbarth, M. Wacker, T. Knobloch, K. Langer and B. Roder, *J Control Release*, 2010, **148**, e117-118.
8. S. Battah, S. Balaratnam, A. Casas, S. O'Neill, C. Edwards, A. Batlle, P. Dobbin and A. J. MacRobert, *Mol Cancer Ther*, 2007, **6**, 876-885.
9. C. V. Synatschke, T. Nomoto, H. Cabral, M. Fortsch, K. Toh, Y. Matsumoto, K. Miyazaki, A. Hanisch, F. H. Schacher, A. Kishimura, N. Nishiyama, A. H. Muller and K. Kataoka, *ACS Nano*, 2014, **8**, 1161-1172.
10. M. Guo, H. Mao, Y. Li, A. Zhu, H. He, H. Yang, Y. Wang, X. Tian, C. Ge, Q. Peng, X. Wang, X. Yang, X. Chen, G. Liu and H. Chen, *Biomaterials*, 2014, **35**, 4656-4666.
11. M. Gary-Bobo, O. Hocine, D. Brevet, M. Maynadier, L. Raehm, S. Richeter, V. Charasson, B. Looock, A. Morere, P. Maillard, M. Garcia and J. O. Durand, *Int J Pharm*, 2012, **423**, 509-515.
12. S. Hackbarth, V. Horneffer, A. Wiehe, F. Hillenkamp and B. Röder, *Chem. Phys.*, 2001, **269**, 339-346.
13. C. C. Lee, J. A. MacKay, J. M. Frechet and F. C. Szoka, *Nat Biotechnol*, 2005, **23**, 1517-1526.
14. L. M. Kaminskas, B. J. Boyd and C. J. Porter, *Nanomedicine (Lond)*, 2011, **6**, 1063-1084.
15. E. R. Gillies and J. M. Frechet, *Drug Discov Today*, 2005, **10**, 35-43.
16. N. Nishiyama, H. R. Stapert, G. D. Zhang, D. Takasu, D. L. Jiang, T. Nagano, T. Aida and K. Kataoka, *Bioconjug Chem*, 2003, **14**, 58-66.
17. N. Nishiyama, Y. Nakagishi, Y. Morimoto, P. S. Lai, K. Miyazaki, K. Urano, S. Horie, M. Kumagai, S. Fukushima, Y. Cheng, W. D. Jang, M. Kikuchi and K. Kataoka, *J Control Release*, 2009, **133**, 245-251.
18. C. Kojima, Y. Toi, A. Harada and K. Kono, *Bioconjug Chem*, 2007, **18**, 663-670.
19. A. Francois, S. Battah, A. J. MacRobert, L. Bezdetsnaya, F. Guillemin and M. A. D'Hallewin, *BJU Int*, 2012, **110**, E1155-1162.
20. E. Yeow, K. Ghiggino, J. Reek, M. Crossley, A. Bosman, A. Schenning and E. Meijer, *J. Phys. Chem. B*, 2000, **104**, 2596-2606.
21. M. Trester-Zedlitz, K. Kamada, S. K. Burley, D. Fenyo, B. T. Chait and T. W. Muir, *J Am Chem Soc*, 2003, **125**, 2416-2425.
22. J. A. Hargus, F. R. Fronczek, M. G. Vicente and K. M. Smith, *Photochem Photobiol*, 2007, **83**, 1006-1015.
23. D. M. Sweet, R. B. Kolhatkar, A. Ray, P. Swaan and H. Ghandehari, *J Control Release*, 2009, **138**, 78-85.
24. S. Hackbarth, J. Schlothauer, A. Preuss and B. Röder, *Laser Phys Lett*, 2013, **10**.
25. F. Wilkinson, W. P. Helman and A. B. Ross, *J Phys Chem Ref Data*, 1993, **22**, 113-262.

26. R. G. Malgady and D. B. Krebs, *Phys Ther*, 1986, **66**, 110-120.
27. R. Taylor, *J Diagn Med Sonogr.*, 1990, **6**, 35-39.
28. J. Megow, M. I. Rohr, M. Schmidt am Busch, T. Renger, R. Mitric, S. Kirstein, J. P. Rabe and V. May, *Phys Chem Chem Phys*, 2015, **17**, 6741-6747.
29. A. Kay, R. Humphry-Baker and M. Grätzel, *J. Phys. Chem.*, 1994, **98**, 952-959.
30. P. Li, G. Zhou, X. Zhu, G. Li, P. Yan, L. Shen, Q. Xu and M. R. Hamblin, *Photodiagnosis Photodyn Ther*, 2012, **9**, 76-82.
31. H. Park and K. Na, *Biomaterials*, 2013, **34**, 6992-7000.
32. G. D. Zhang, A. Harada, N. Nishiyama, D. L. Jiang, H. Koyama, T. Aida and K. Kataoka, *J Control Release*, 2003, **93**, 141-150.
33. E. C. Cho, Q. Zhang and Y. Xia, *Nat Nanotechnol*, 2011, **6**, 385-391.
34. Y. Li, M. Kroger and W. K. Liu, *Biomaterials*, 2014, **35**, 8467-8478.
35. H. Hatakeyama, H. Akita and H. Harashima, *Adv Drug Deliv Rev*, 2011, **63**, 152-160.
36. D. Kessel and Y. Luo, *J Photochem Photobiol B*, 1998, **42**, 89-95.
37. M. H. Teiten, L. Bezdetnaya, P. Morliere, R. Santus and F. Guillemin, *Br J Cancer*, 2003, **88**, 146-152.
38. H. Mojzisoava, S. Bonneau, C. Vever-Bizet and D. Brault, *Biochim Biophys Acta*, 2007, **1768**, 2748-2756.
39. U. Schmidt-Erfurth, H. Diddens, R. Birngruber and T. Hasan, *Br J Cancer*, 1997, **75**, 54-61.
40. N. S. Soukos, M. R. Hamblin and T. Hasan, *Photochem Photobiol*, 1997, **65**, 723-729.
41. J. D. Spikes, *J Photochem Photobiol B*, 1990, **6**, 259-274.
42. K. Feldman, G. Hahner, N. Spencer, P. Harder and M. Grunze, *J Am Chem Soc*, 1999, **121**, 10134-10141.
43. A. Yuan, B. Yang, J. Wu, Y. Hu and X. Ming, *Acta Biomater*, 2015.
44. D. Shcharbin, J. Mazurb, M. Szwedzka, M. Wasiak, B. Palecz, M. Przybyszewska, M. Zaborski and M. Bryszewskaa, *Colloids and Surfaces B: Biointerfaces*, 2007, **58**, 286-289.
45. M. Lundqvist, J. Stigler, G. Elia, I. Lynch, T. Cedervall and K. A. Dawson, *Proc Natl Acad Sci U S A*, 2008, **105**, 14265-14270.
46. J. L. Perry, K. G. Reuter, M. P. Kai, K. P. Herlihy, S. W. Jones, J. C. Luft, M. Napier, J. E. Bear and J. M. DeSimone, *Nano Lett*, 2012, **12**, 5304-5310.
47. C. D. Walkey, J. B. Olsen, H. Guo, A. Emili and W. C. Chan, *J Am Chem Soc*, 2011, **134**, 2139-2147.
48. O. P. Perumal, R. Inapagolla, S. Kannan and R. M. Kannan, *Biomaterials*, 2008, **29**, 3469-3476.
49. J. D. Trono, K. Mizuno, N. Yusa, T. Matsukawa, K. Yokoyama and M. Uesaka, *J Radiat Res*, 2011, **52**, 103-109.
50. F. R. Maxfield and T. E. McGraw, *Nat Rev Mol Cell Biol*, 2004, **5**, 121-132.
51. R. G. Parton and K. Simons, *Nat Rev Mol Cell Biol*, 2007, **8**, 185-194.
52. G. Sahay, J. O. Kim, A. V. Kabanov and T. K. Bronich, *Biomaterials*, 2010, **31**, 923-933.
53. M. Kress, T. Meier, R. Steiner, F. Dolp, R. Erdmann, U. Ortmann and A. Ruck, *J Biomed Opt*, 2003, **8**, 26-32.
54. H. P. Lassalle, M. Wagner, L. Bezdetnaya, F. Guillemin and H. Schneckenburger, *J Photochem Photobiol B*, 2008, **92**, 47-53.
55. Y. Li, H. T. Duong, S. Laurent, A. MacMillan, R. M. Whan, L. V. Elst, R. N. Muller, J. Hu, A. Lowe, C. Boyer and T. P. Davis, *Adv Healthc Mater*, 2015, **4**, 148-156.



Scheme 1: Synthetic route for the preparation of di-amino PEG-functionalized chlorin 2.
254x100mm (96 x 96 DPI)



Scheme 2: Synthetic route to multifunctional PAMAM dendritic NPs 3 and 4.
254x190mm (96 x 96 DPI)

Table 1: Photophysical properties

Photosensitizer system	λ_{\max} (nm) (Q-absorption)	λ_{\max} (nm) (fluorescence)	Φ_{FL} (± 0.05) (fluorescence)	Φ_{Δ} (± 0.02) (singlet oxygen)	Hydrodynamic Diameter (nm) /PDI	Zeta potential (mV)
Ce6	662.5	669	0.16	0.55	N.A.	N.A.
G4.5-Ce6	665	670.5	0.11	0.26	6.3/0.23	-17.7
G4.5-Ce6-PEG	664.5	671.5	0.09	0.31	12/0.33	-8.9

λ_{\max} : Maximal wavelength of absorption and fluorescence (excitation wavelength: 410 nm) in the last Q-band of the visible spectrum in ethanol.

Φ_{Δ} : Singlet oxygen quantum yield.

Φ_{FL} : Fluorescence quantum yield.

Since the fluorescence quantum yield and singlet oxygen quantum yield are determined by comparison with a known reference, the error is mainly caused by the error of the reference, and thus it has the same percentage for all samples.

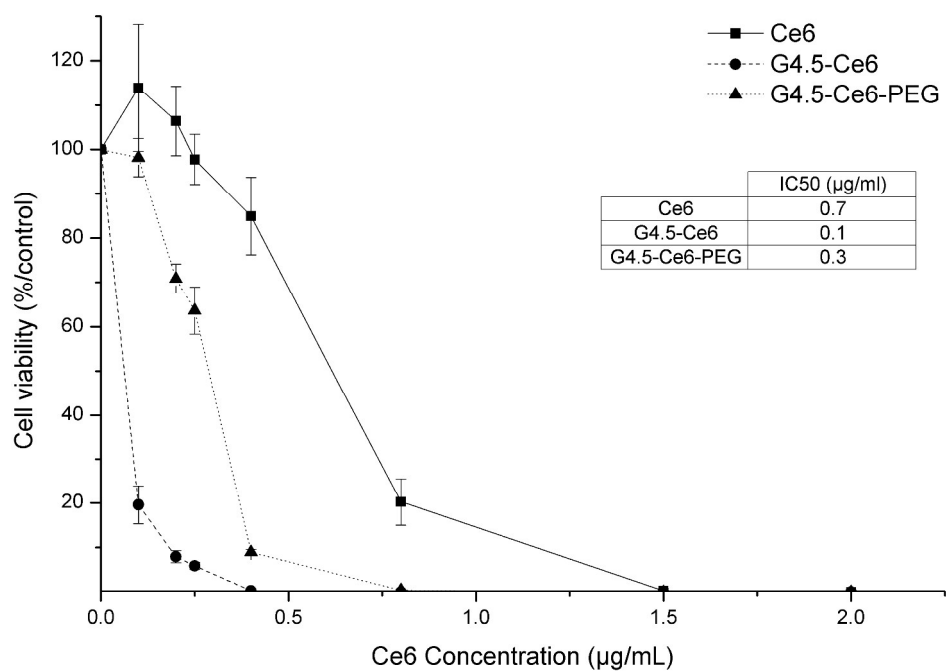


Fig. 2: In vitro antitumor activity of free Ce6 (square), G4.5-Ce6 (round) and G4.5-Ce6-PEG (triangle) after photoirradiation ($2.5 \text{ J}\cdot\text{cm}^{-2}$). FaDu cells were treated 24h with various concentrations of free Ce6 or vectorized with G4.5 dendrimers (+/-PEG). IC50: Concentration of the PS inducing 50% of cell death.
297x207mm (300 x 300 DPI)

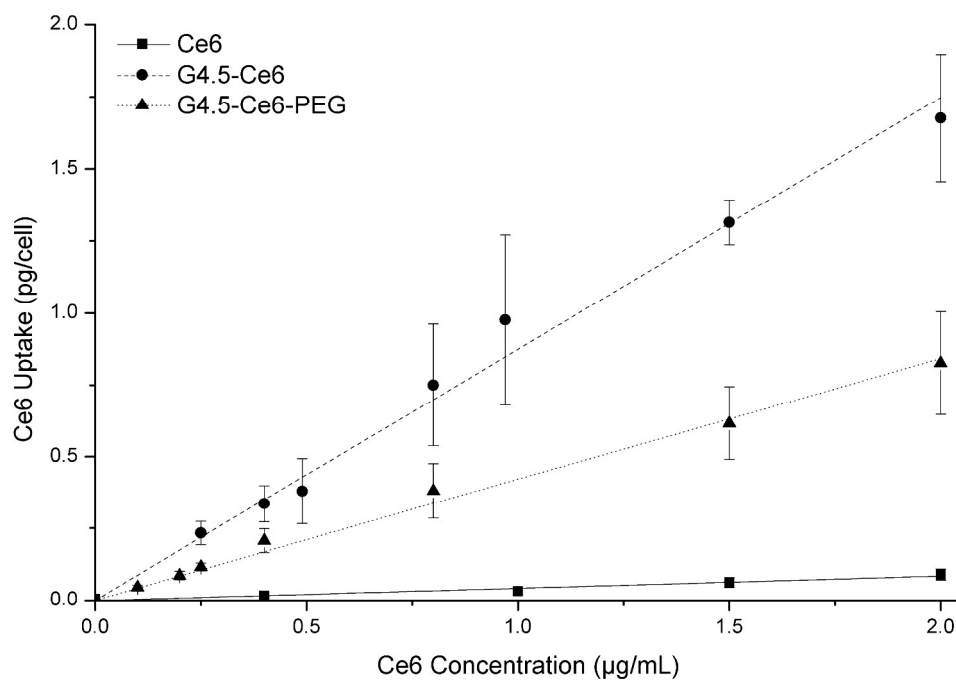


Fig. 3: Cellular uptake of free Ce6 (square), G4.5-Ce6 (round) and G4.5-Ce6-PEG (triangle) incubated with FaDu cells during 24h as function of the PS concentration.
297x207mm (300 x 300 DPI)

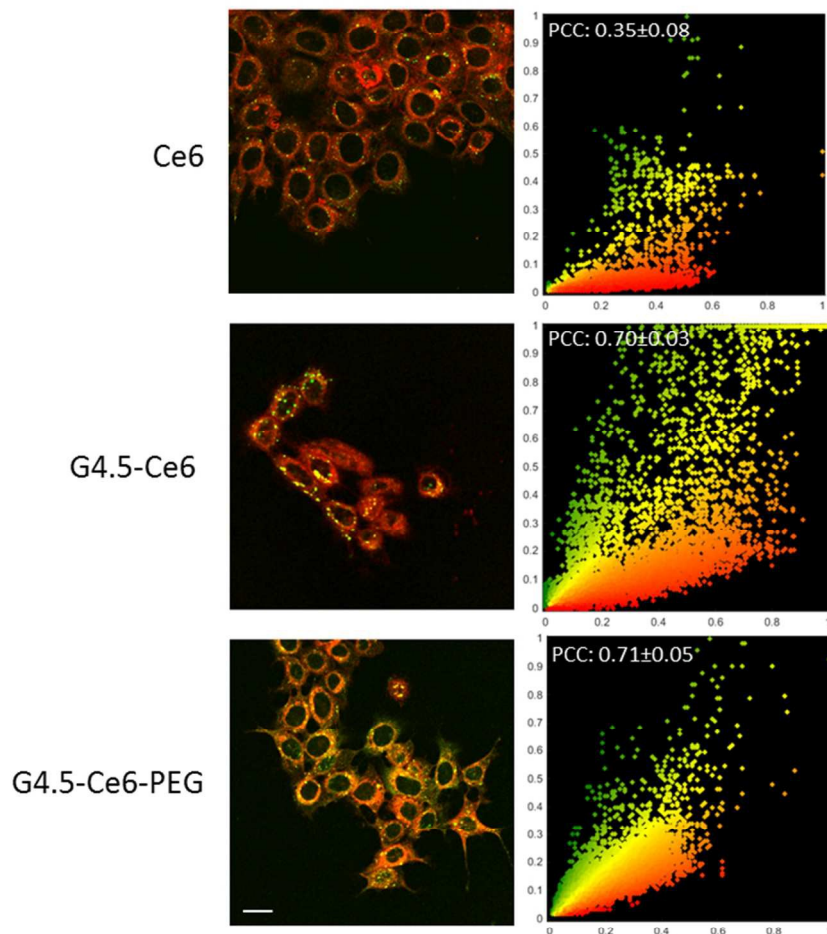


Fig. 4a: CLSM images of lysosomal localization of Ce6, G4.5-Ce6 and G4.5-Ce6-PEG in FaDu cells. Left column display confocal overlay images. These micrographs were representative of those obtained from three independent experiments. Right column shows the mean Pearson's correlation diagram. Red color corresponds to Ce6 and green color corresponds to LysoTracker® Green. Bar = $10\mu\text{m}$
219x239mm (96 x 96 DPI)

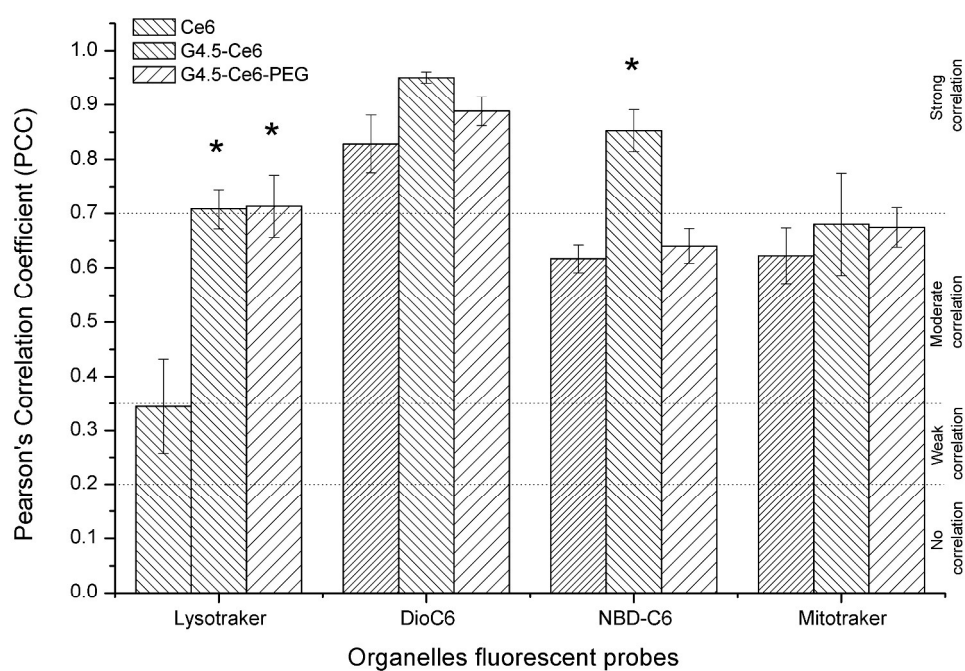


Fig. 4b: Pearson's correlation coefficient (PCC) values quantifying the co-localization of the organelles fluorescent marker and free Ce6, G4.5-Ce6 or G4.5-Ce6-PEG in FaDu cells 24 h after incubation. PCC values of 1-0.7 indicate a relatively strong correlation, 0.69-0.36 indicate a moderate correlation, 0.35-0.2 indicate a weak correlation, and <0.2 indicates the absence of a correlation^{26, 27}. (* $p < 0.05$ versus the free Ce6 group).

297x207mm (300 x 300 DPI)

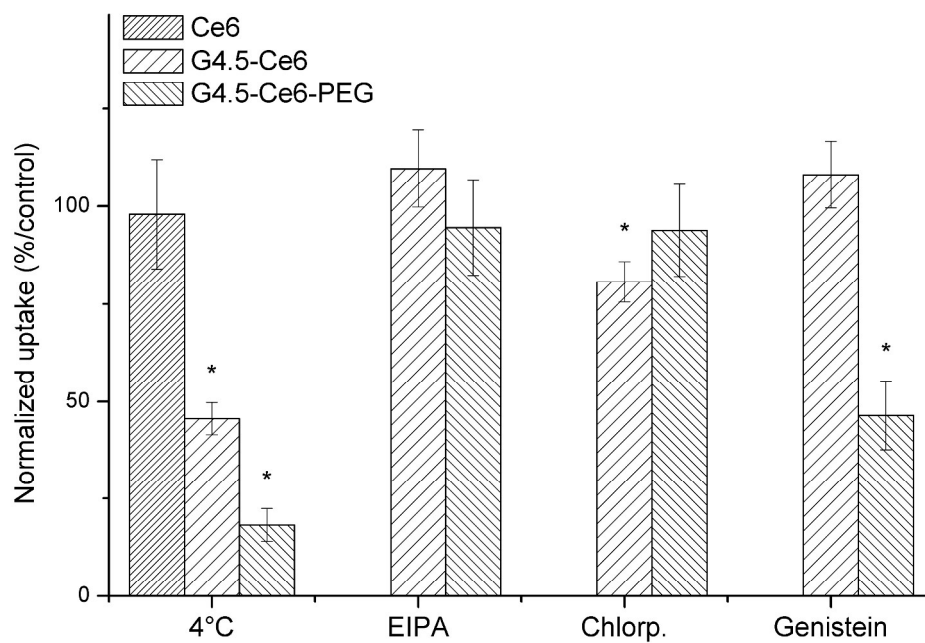


Fig. 5: Effect of various endocytosis inhibitors on cellular uptake of the PSs. FaDu cells were pre-incubated for 30 min at 4°C without the endocytosis inhibitors or at 37°C with inhibitors. After pre-incubation, PSs (final concentration 0.5 $\mu\text{g}\cdot\text{ml}^{-1}$) were added and incubated for 60 min, either in the presence of the inhibitors or at 4°C. (* $p < 0.05$ versus the untreated control group).

297x207mm (300 x 300 DPI)

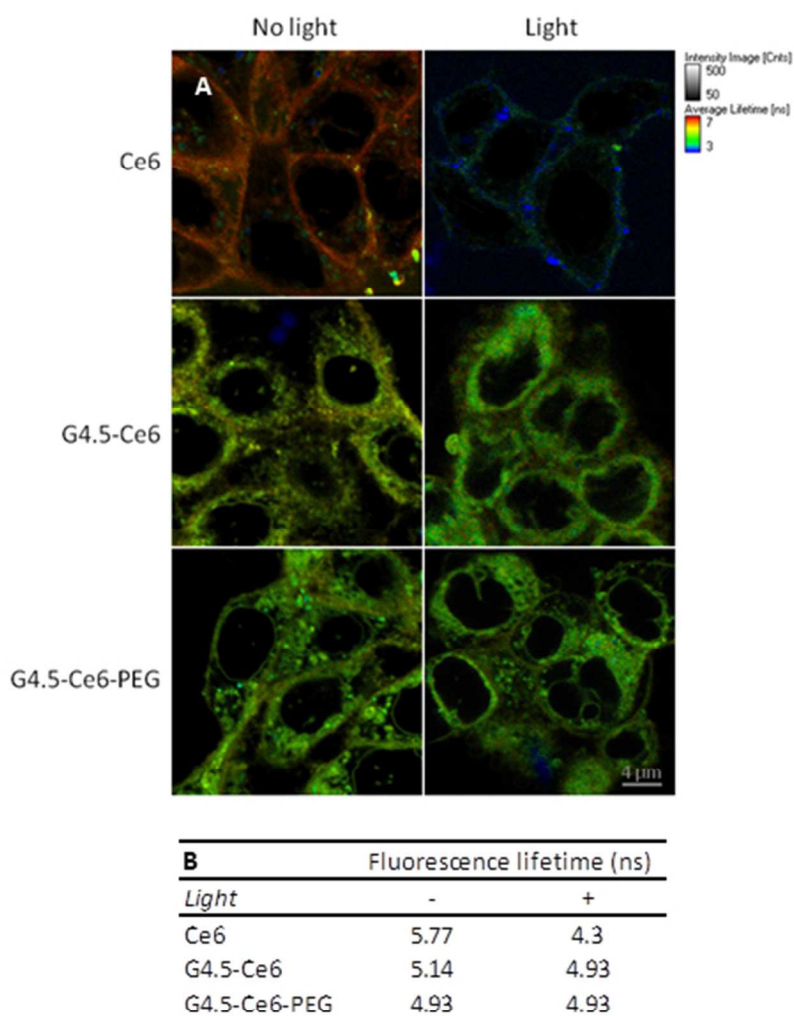
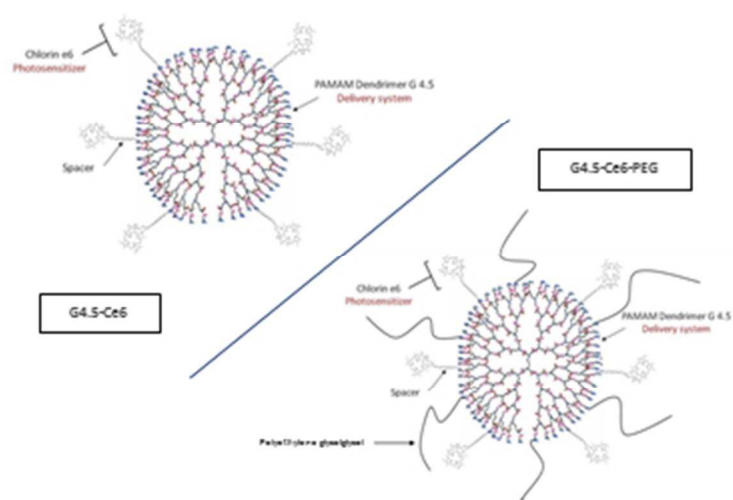


Fig. 6: Representation of fluorescence lifetime imaging microscopy (FLIM). FaDu cells were treated with 3 μM of free Ce6, G4.5-Ce6 or G4.5-Ce6-PEG. After 24h, the cells were observed under a fluorescence-lifetime imaging microscope before and after irradiation (a). Average fluorescence lifetimes for each PSs were determined (b).

129x179mm (96 x 96 DPI)



Covalent conjugates between the photosensitizer chlorin e6 and PAMAM G4.5 dendrimers
100x69mm (96 x 96 DPI)